Since January 2020 Elsevier has created a COVID-19 resource centre with free information in English and Mandarin on the novel coronavirus COVID-19. The COVID-19 resource centre is hosted on Elsevier Connect, the company's public news and information website.

BASIC SCIENCE

Nanomedicine: Nanotechnology, Biology, and Medicine
34 (2021) 102372

Original Article

nanomedjournal.com

Synthesis and immunogenicity assessment of a gold nanoparticle conjugate for the delivery of a peptide from SARS-CoV-2

Susan Farfán-Castro[a,b,1], Mariano J. García-Soto[a,1], Mauricio Comas-García[b,c], Jaime I. Arévalo-Villalobos[b], Gabriela Palestino[a,b], Omar González-Ortega[a,*], Sergio Rosales-Mendoza[a,b,*]

[a]*Facultad de Ciencias Químicas, Universidad Autónoma de San Luis Potosí, SLP, Mexico*
[b]*Centro de Investigación en Ciencias de la Salud y Biomedicina, Universidad Autónoma de San Luis Potosí, SLP, Mexico*
[c]*Facultad de Ciencias, Universidad Autónoma de San Luis Potosí, SLP, Mexico*

Revised 24 December 2020

Abstract

The development of vaccines is a crucial response against the COVID-19 pandemic and innovative nanovaccines could increase the potential to address this remarkable challenge. In the present study a B cell epitope ($S_{461\text{-}493}$) from the spike protein of SARS-CoV-2 was selected and its immunogenicity validated in sheep. This synthetic peptide was coupled to gold nanoparticles (AuNP) functionalized with SH-PEG-NH_2 via glutaraldehyde-mediated coupling to obtain the AuNP-$S_{461\text{-}493}$ candidate, which showed in s.c.-immunized mice a superior immunogenicity (IgG responses) when compared to soluble $S_{461\text{-}493}$; and led to increased expression of relevant cytokines in splenocyte cultures. Interestingly, the response triggered by AuNP-$S_{461\text{-}493}$ was similar in magnitude to that induced using a conventional strong adjuvant (Freund's adjuvant). This study provides a platform for the development of AuNP-based nanovaccines targeting specific SARS-CoV-2 epitopes.

Key words: Nanovaccine; COVID-19; Humoral response; Antigen carrier; Adjuvant

The new coronavirus, SARS-CoV-2, affecting human health is leading to devastating effects in terms of morbidity, mortality, and economic impact.[1] In response to this emergency, the development of vaccines has been rapidly implemented and thus far at least ten candidates have reached phase III clinical trials and about forty are under phase I/II evaluations.[2,3] Most of the candidates target the spike protein (S), which is a critical target to achieve virus neutralization through antibodies by preventing its entry into the host cell.[4,5] The protein S has also been associated with the induction of cellular responses of relevance for clearance of infected cells.[6] Most of the vaccine candidates are formulated with the full-length protein S and based on viral vectors or inactivated viruses. Such formulations, although highly immunogenic, could be associated to side effects such as high reactogenicity and the induction of suboptimal, if not unsafe, immune responses.[2,4,5,7]

The rational design of vaccines should be rapidly implemented in the case of SARS-CoV-2 to produce the next generation vaccines as an alternative path for the induction of optimal immune responses. The possible critical points in this regard are the induction of robust neutralizing humoral responses that avoid the induction of antibodies that act as antibody-dependent enhancement inducers.[8,9] An approach to achieve such goals relies in the use of epitope-based vaccines formulated with synthetic peptides, which allow focusing the response on the particular epitopes that induce neutralizing antibodies.[10] Therefore, epitope-based vaccines are proposed as fine vaccine formulations capable of achieving the optimal immune responses.[4,9] However, the use of such simplified antigenic formulations compared to whole virus-based vaccines imposes the challenge of achieving robust immunogenicity, which is

Acknowledgments: This work was supported by Consejo Nacional de Ciencia y Tecnología (CONACyT, grant 311879 to SRM, and grant A1-S-31287 to GP), Consejo Potosino de Ciencia y Tecnología (COPOCyT, grant FIIS-FS04-19), and Programa para el Desarrollo Profesional Docente (PRODEP, grant UASLP-PTC-625 to MJGS).

* Corresponding authors at: Facultad de Ciencias Químicas, Universidad Autónoma de San Luis Potosí, SLP, Mexico.
E-mail addresses: omar.gonzalez@uaslp.mx, (O. González-Ortega), rosales.s@uaslp.mx. (S. Rosales-Mendoza).
[1] Contributed equally to this work.

https://doi.org/10.1016/j.nano.2021.102372
1549-9634/

often remediated by the inclusion of adjuvants and/or carriers to enhance vaccine immunogenicity by several mechanisms.[5,7,11]

Among the nanocarriers used for this purpose, gold nanoparticles (AuNP) are promising agents since they exert reduced toxicity and are apt to functionalization with antigens.[12,13] Some of the molecular mechanisms that are behind the application of AuNP as antigen carriers have been described. For instance, it is known that AuNP are efficiently captured by dendritic cells and this process is improved if they are covered with polyethylene glycol at a reasonable graft density[14]; cellular internalization occurs by phagocytosis, macropinocytosis and receptor-mediated endocytosis in dendritic cells and is largely dependent on the physicochemical properties of AuNP, determined by the size and surface modification of the particles.[15,16] Once internalized, the peptides are loaded onto MHC molecules and expressed on the cell surface to be presented to lymphocytes.[17]

It is known that AuNP-antigen conjugates increase the antigen presentation process[18] by promoting the effective maturation of dendritic cells and proliferation of Th and NK cells, achieving an increased secretion of cytokines IL-4, IFNg, IL-12 and IL-10.[16,19]

A recent review has covered the outlook on the application of nanomaterials for the development of vaccines against SARSCoV-2, highlighting the potential of some previously reported vaccines against other viruses based on metallic particles, including AuNP.[20] In fact, previous efforts have been reported on the development of AuNP-based vaccine against coronavirus, but optimization in the formulation is required given the limited neutralization potential and some concerns derived from the use of full-length protein S, which might induce a suboptimal humoral response[21] . Thus far, the preclinical evaluation of several AuNP-based vaccines has been reported with promising findings.[20–23] Therefore, AuNP-based vaccines forecast a promising path for the development of rationally designed subunit vaccines. Herein, a peptide derived from the SARS-CoV-2 protein S sequence was successfully coupled to AuNP and the bioconjugate obtained was characterized and used to assess its immunogenic potential in mice.

Materials and methods

Antigen selection

The $S_{461\text{-}493}$ peptide was selected from the sequence of the motif binding domain of the protein S ($S_{437\text{-}508}$), which contains several potential B cell epitopes predicted by the BepiPred-2.0: Sequential B-Cell Epitope Predictor tool. $S_{461\text{-}493}$ has a reasonable size to be obtained by chemical synthesis. In addition, a cysteine was included at the N-terminus of the peptide to facilitate its eventual attachment to carriers via the thiol group. The final sequence of the $S_{461\text{-}493}$ peptide was: CLKPFERDISTEIYQAGSTPCNGVEGFNCYFPLQ, synthesized by Synpeptide Inc.(Shanghai, China).

Preparation of the KLH-$S_{461\text{-}493}$ conjugate and production of anti-serum

The $S_{461\text{-}493}$ peptide was conjugated to the keyhole limpet hemocyanin (KLH; Geno Technology Inc., St. Louis, MO) carrier using ethyl-3-[3-dimethylaminopropyl] carbodiimide (EDC). The reaction was performed according to the instructions from the manufacturer (Thermo Fisher Scientific, Waltham, MA), with some modifications comprising 500 μg of peptide and 1 mg of KLH, reacted with EDC previously dissolved in DMSO. The reaction conditions and purification of the conjugate were performed according to a previous report.[24]

The protocols involving test animals were performed according to the Guide for the Care and Use of Laboratory Animals of the National Institutes of Health (NIH, Bethesda, MD) and protocols approved by the Institutional Research Ethics Committee (CEID-2020-07R1). A 12-month-old female sheep (Ramboiullet breed) was immunized four times at 2-week intervals with the KLH-$S_{461\text{-}493}$ conjugate (250 μg). The antigen was emulsified in Complete Freund's Adjuvant (CFA) for priming and incomplete Freund's adjuvant (IFA) for boosting. Blood samples were obtained by jugular puncture, and the recovered sera were stored at −40 °C until further use.

ELISA analysis

The levels of anti-$S_{461\text{-}493}$ antibodies were determined from the sheep sera samples by ELISA, which comprised coating, overnight at 4 °C, 96-well polystyrene plates with the $S_{461\text{-}493}$ peptide (400 ng/well) diluted in carbonate buffer (15 mM Na_2CO_3 and 35 mM $NaHCO_3$). The plates were washed three times with PBS-T at each stage of the assay. The blocking step comprised a 2 h incubation with 5% fat-free milk at 25 °C. Serial dilution of the test sera was applied to the plate followed by incubation overnight at 4 °C. Secondary labeling was performed at 25 °C for 2 h using a donkey horseradish peroxidase-conjugated anti-sheep IgG (1:10,000 dilution, Sigma-Aldrich, St. Louis, MO). An ABTS substrate solution containing 0.6 mM 2,2′-azino-bis (3-ethylbenzothiazoline-6-sulfonic acid) (ABTS; Sigma-Aldrich), 0.1 M citric acid, and 1 mM H_2O_2 at pH 4.35 was used for the detection. After 30 min of incubation at 25 °C, OD values at 405 nm were recorded with a Multiskan FC microplate photometer (Thermo Fisher Scientific, Waltham, MA).

Synthesis, functionalization, and conjugation of AuNP

Gold (III) chloride hydrate (99.995%), sodium citrate tribasic dihydrate (≥ 99.5%), thiol-poly(ethylene glycol)-amine (M_n 5000), glutaraldehyde (25% in H_2O), and sodium borohydride (≥99%) were purchased from Sigma-Aldrich (St Louis, MO) and used as received. The synthesis of AuNP is described first, and the functionalization with HS-PEG-NH_2 and conjugation with peptide $S_{461\text{-}493}$ afterwards (Scheme 1).

For the synthesis of AuNP, all glassware was cleaned with aqua regia and rinsed thoroughly with deionized water.[25] Stock solutions of 1% $HAuCl_4$ and 1% $Na_3C_6H_5O_7$ were prepared with Milli-Q water one day before their use. A reaction mixture containing 0.25% $HAuCl_4$, 0.25% $Na_3C_6H_5O_7$, and water was prepared by adding each component in sequence and under mixing. This mixture was incubated for 5 min and added rapidly to a flask with water already boiling for a final concentration of 0.01% $HAuCl_4$ and 0.01% $Na_3C_6H_5O_7$. Reflux occurred for 30 min. The as-prepared AuNP were stored at 4 °C.

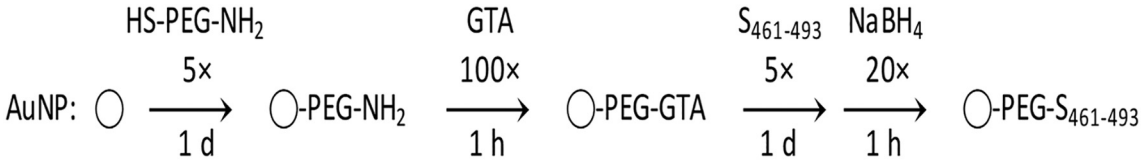

Scheme 1. Functionalization of AuNP with HS-PEG-NH_2 and conjugation with $S_{461-493}$ using glutaraldehyde (GTA) as crosslinker.

For the functionalization of AuNP, the amount of HS-PEG-NH_2 was calculated considering a grafting density of one molecule covering 2 nm[2,26] Per 1 mL of as-prepared AuNP, 5 μL of 1 M HCl was added first, followed by HS-PEG-NH_2 five times in excess (equivalent to form five monolayers of PEG per AuNP), and 2 μL of 5% Tween 20 while stirring. This solution was mixed 1 h at 4 rpm and left undisturbed overnight. The particles were washed twice by centrifuging 10 min at 20,000 ×*g* and replacing the original volume of supernatant with phosphate-buffered saline (PBS) 1× containing 0.01% Tween 20 (PBST).

For the conjugation of AuNP-PEG-NH_2, the same grafting density as described above was considered. First, glutaraldehyde (GTA) was added 100 times in excess, the solution mixed for 1 h at 4 rpm, and the particles washed as described. Afterwards, the $S_{461-493}$ peptide dissolved in DMSO was added 5 times in excess, the solution mixed overnight at 4 rpm, and the particles washed as described. Finally, sodium borohydride was added 20 times in excess, the solution mixed for 1 h at 4 rpm, and the particles washed as described. The unreacted $S_{461-493}$ peptide was quantified via HPLC. A C18 column of 15 cm × 0.5 cm (L × I.D.) was used with a linear gradient method starting from solution A (0.1% trifluoroacetic acid in water) and changing to solution B (0.1% trifluoroacetic acid in acetonitrile) during 10 min, with a flow rate of 0.6 mL/min. 50 μL of sample was injected, carrying out the detection at 214 nm.

The particles were characterized after every reaction step, measuring their absorbance in the visible region with a spectrophotometer Jenway 6705 (Bibby Ltd., Stone, UK), and their size and ζ potential with a zetasizer Nano ZS (Malvern Ltd., Malvern, UK) equipped with a 633-nm laser and a 173° backscatter detector. The ionic strength of the solution containing the as-prepared AuNP was 5.3 mM, and that of the PBS 1× solution where the functionalized and conjugated AuNP were resuspended was 0.17 M. The variations in net charge were compared using electrophoresis, with 4:1 (v:v) mixtures of 10×-concentrated AuNP and 30% glycerol deposited in a 0.75% agarose gel.[27] The gel was prepared with Tris-acetate-EDTA (TAE) 1× buffer, casted and immersed horizontally in a chamber with TA 1× buffer at pH 7, and run for 30 min at 100 V.

TEM analysis

The size and morphology of the AuNP before and after conjugation were determined using a JEM-JEOL-2100 Transmission Electron Microscope at 200 kV. The AuNP suspension was diluted until the first dilution became colorless. Afterwards, 5 μL of sample was deposited on a nickel formvar/carbon coated grid (Ted Pella Inc) for 1 min, washed with Milli-Q water, and left to dry for 24 h in a desiccator. The conjugated AuNP were analyzed using the aforementioned method and also by negatively staining them with 1% uranyl acetate. The size distribution was calculated using at least 100 measurements of the average diameter. The diameter of each particle was estimated from the geometric mean of two orthogonal measurements.

Cytotoxicity evaluation

The cytotoxicity of the different conjugates was evaluated using trypan blue staining and the resazurin assay. HEK-293T cells were grown in DMEM (Corning Inc., Corning, NY) supplemented with ampicillin/streptomycin (Thermo Fisher Scientific), and 10% heat-inactivated fetal bovine serum (Gibco®) at 37 °C and 5% CO_2 using T75 flasks (Corning) until reaching confluence. One day before the cytotoxicity evaluation, 1×10^5 cells were seeded by triplicate in a 12-well culture plate. Each experiment was done with two different cell passages. As controls each plate had cells treated with the vehicle alone or H_2O_2 (40 mM). The cells were subsequently exposed to different concentrations of AuNP (12.5-250 μg/mL) during 48 h under the aforesaid culture conditions. Afterwards, the cells were detached from the plates by pipetting and 100 μL of the suspension was mixed with 100 μL of 0.4% trypan blue (Sigma-Aldrich) and incubated for 2 min; 10 μL aliquots were loaded in a Neubauer hemocytometer. The number of cells was determined using a Primovert inverted microscope under the 40× objective (Carl Zeiss AG, Jena, Germany). The number of live and dead cells was determined by averaging cells from each quadrant (large corner squares on the 0.25 × 0.25 mm grid) of each chamber and multiplied by 2 (dilution factor) and 10,000 (correction factor). The live cells are round and cause Newton's rings, while the death cells are not usually round but blue and non-refractile. As per protocol, cells touching the edge of the squares were not counted. The number of total cells in the experimental wells was normalized with respect to the cells treated with the vehicle alone.

In parallel, the resazurin-based cell viability was estimated. For this purpose, the cells treated during 48 h with the respective AuNP concentrations were exposed to 30 μg/mL resazurin for 3 h and fluorescence (560 nm/590 nm) was recorded in a FlexStation II scanning fluorimeter (Molecular Devices LLC, San Jose, CA).

Immunogenicity assessment

Test mice (BALB/c strain, 8-10 weeks old) groups were established randomly ($n = 5$). The immunization scheme comprised the administration of three subcutaneous doses (100 μL) on days 0, 14, and 21. Mice received one of the following treatments: $S_{461-493}$ peptide (5 μg) diluted in PBS, $S_{461-493}$ peptide plus complete Freund's adjuvant (for priming,

while for boosting the incomplete version was used), a low dose of AuNP-$S_{461\text{-}493}$ (corresponding to 0.5 μg of $S_{461\text{-}493}$), or a high dose of AuNP-$S_{461\text{-}493}$ (corresponding to 5 μg of $S_{461\text{-}493}$). Blood samples (0.2 mL) were collected by tail puncture on days 0, 13, 27, and 41. After clotting they were centrifuged at 1200 ×*g* for 10 min and the sera separated and stored at −20 °C until further analysis.

Anti-$S_{461\text{-}493}$ antibody levels were determined by ELISA. The plates were coated with the $S_{461\text{-}493}$ peptide (400 ng per well) diluted in 0.2 M carbonate buffer (pH 9.6) and incubated overnight at 4 °C. Each incubation step was preceded by three washes with PBST (PBS 1× + 0.05% Tween 20). The plates were blocked with a fat-free powder milk solution (5%) at room temperature during 2 h. Serial dilutions of the test sera were applied and incubated overnight at 4 °C. Horseradish peroxidase-conjugated anti-mouse IgG (1:2000 dilution; Sigma-Aldrich), IgM, IgG1, or IgG2a was used for secondary labeling, which comprised a 2 h incubation at 25 °C. The reaction was developed by adding a substrate solution of 0.3 mg/L ABTS and 0.1 M H_2O_2, followed by a 20 min incubation at 25 °C. OD_{405} values were measured in a Multiskan Ascent microplate reader (Thermo Fisher Scientific). Statistical significance (*P* values) was determined using one-way ANOVA. Statistical analysis was performed with Statistica® 12.7 (TIBCO Software Inc., Palo Alto, CA).

Cytokine transcriptome analysis

Two test mice treated with the AuNP-$S_{461\text{-}493}$ vaccine were sacrificed and the isolation of splenocytes was performed under standard methods. The spleen was isolated and placed into a cell strainer fitted on a 50 mL tube. The organ was pressed with a 1 mL syringe plunger while adding and 5 mL of culture medium (RPMI containing 10% FBS and 1% pen-strep) to release the cells. The cells' suspension was spun at 1500 rpm for 5 min and resuspended in 3 mL lysis buffer (8.3 g/L NH_4Cl, 10 mM Tris–HCl, pH 7.4) and incubated for 5 min at 37 °C. Cells were washed twice with RPMI containing 1% pen-strep medium and finally resuspended in RPMI with 10% FBS and 1% pen-strep. Cell viability was estimated using the trypan blue method and if this parameter was above 95% the cells were used to set the stimulation protocol. 1×10^6 cells were placed in 12-well plates and treated with 5 μg/mL $S_{461\text{-}493}$ peptide or the vehicle alone (with PBS as control). The cell cultures were incubated for 72 h at 37 °C under 5% CO_2. The total RNA from splenocytes was isolated using TRIzol® reagent (Invitrogen, Waltham, MA) following the manufacturer's instructions. The concentration and quality of the extracted RNA were determined using a BioPhotometer 6131 (Eppendorf, Hamburg, Germany). The synthesis of cDNA was subsequently performed using the M-MuLV Reverse Transcriptase kit (New England Biolabs Inc., Ipswich, MA) from 1 μg of total RNA as template and following the manufacturer's instructions. qPCR analysis was performed in a StepOnePlus Real-Time PCR system (Applied Biosystems, Waltham, MA) using a SYBR® Green Master mix (Bio-Rad Inc., Hercules, CA). The amplification protocol comprised the following cycling conditions: 95 °C for 5 min (initial denaturation), 40 cycles at 95 °C for 15 s for denaturation, and 58 °C for 60 s for annealing and extension. The ΔΔCT method was applied to determine the fold change on the expression of the target transcripts,[28] using β-actin as the housekeeping gene. Each sample was run by triplicate. The primer sets used to amplify the target cDNA were: IL-2 (sense 5'TCCAGAACATGCCGCAGAG, antisense 5'-CCTGAGCAGGATGGAGAATTACA), IL-4 (sense 5'-GAAGCCCTACAGACGAGCTCA, antisense 5'-ACAGGAGAAGGGACGCCAT), IL-6 (sense 5'-AAGTGCATCATCGTTGTTCATACA, antisense 5'-CAGAATTGCCATCGTACAACTCTTTTCTCA), IFN-γ (sense 5'-TGGGAGTAGACAAGGTACAACCC, antisense 5'-TCAAGTGGCATAGATGTGGAAGAA) and β-actin (sense 5'-CAATAGTGATGACCTGGCCGT, antisense 5'-AGAGGGAAATCGTGCGTGAC).

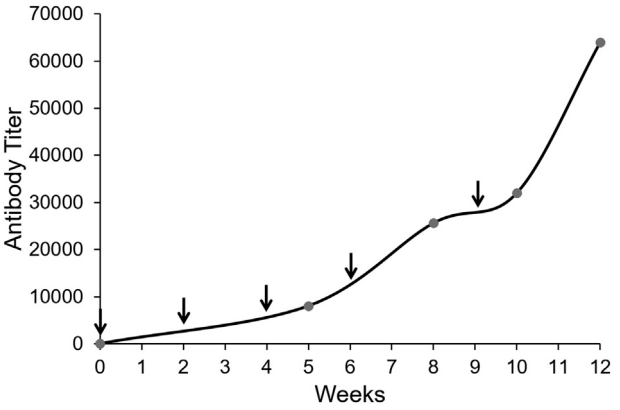

Figure 1. Immunogenicity assessment of the $S_{461\text{-}493}$ peptide in sheep. A 12-month-old female sheep was subjected to a 10-week immunization scheme comprising the s.c. administration of 5 doses of the KLH-$S_{461\text{-}493}$ conjugate (arrows). Anti-$S_{461\text{-}493}$ IgG titers were determined by ELISA at the indicated time points (circles).

Results

Immunogenicity assessment of $S_{461\text{-}493}$ and its conjugation to AuNP

The $S_{461\text{-}493}$ peptide was predicted to carry at least one B cell epitope according to the epitope prediction toll. However, experimental evidence was generated to support the selection of this epitope. The obtained KLH-$S_{461\text{-}493}$ conjugate achieved high titers of antibodies in sheep, confirming the behavior as B cell epitope (Figure 1).

The as-prepared, citrate-coated AuNP had a typical absorbance spectrum with a maximum at 518 nm, as well as a size distribution and ζ potential consistent with previous syntheses. The $S_{461\text{-}493}$ peptide included a cysteine intended for its direct adsorption on the surface of AuNP via the Au-S dative bond (Figure 2, *A*). While not soluble in aqueous buffers or ethanol at 1 mg/mL, the peptide solubilized well in DSMO and was prepared at 30 mg/mL to minimize the amount of DMSO added to the AuNP suspension. However, after testing the peptide with aliquots of as-prepared AuNP at different molecular ratios,[29] all resulted in irreversible aggregates due to the hydrophobic nature

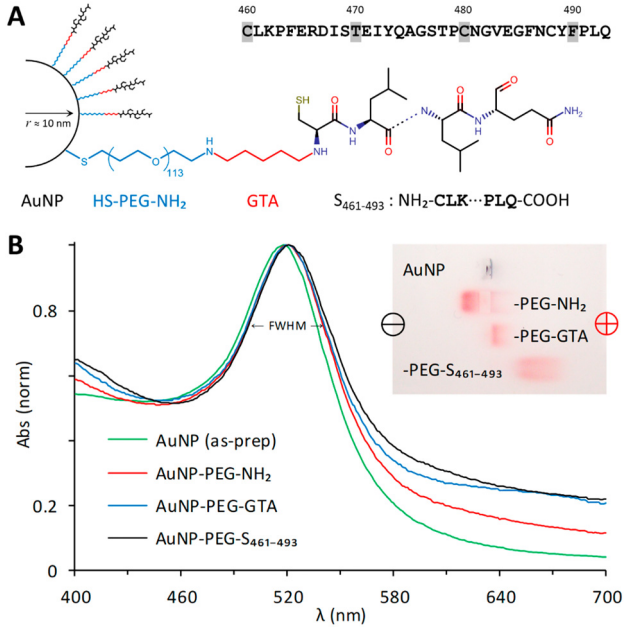

Figure 2. Composition of the AuNP-PEG-$S_{461-493}$ conjugate and characterization during the synthesis. The $S_{461-493}$ peptide was derived from the sequence located at the receptor binding domain of the spike (S) protein from SARS-CoV-2. This peptide was intended as a target antigen and included a cysteine at the N-terminus to facilitate its conjugation to AuNP. Visible spectra and gel electrophoresis of AuNP after their functionalization with HS-PEG-NH_2, activation with glutaraldehyde (GTA), and their conjugation with $S_{461-493}$. The data are representative of five different preparations.

of the peptide and the poor stability of the citrate-coated AuNP against it.

To improve the stability of AuNP we used the bifunctional HS-PEG-COOH and HS-PEG-NH_2, both of M_n 5000 and soluble in aqueous solutions. Either PEG stabilized the AuNP after their functionalization, washing, and resuspension in PBS 1×. Both options allowed exploring different approaches for the conjugation of peptide $S_{461-493}$ to the terminal COOH or NH_2 present on the surface of the PEG-stabilized AuNP. Using the customary EDC/NHS reaction to bind the primary amine of the $S_{461-493}$ peptide to the activated carboxyl group of AuNP-PEG-COOH, we tested one- and two-step conditions in buffers such as 0.2 M PB, PBS 1×, or 0.1 M MES.[30,31] However, while the reaction with all the reactants added in one-step resulted in conjugates that contrasted better, compared to pre-activating and then conjugating, the results were not reproducible due to the highly labile EDC (data not shown). Moreover, both the activated and the conjugated AuNP-PEG-COOH, ended with nearly the same properties than the functionalized AuNP, indicating the predominance of unreacted COOH groups.

Using the amine-reactive crosslinker glutaraldehyde (GTA) to conjugate the primary amine of peptide $S_{461-493}$ to the aldehyde groups obtained after the activation of AuNP-PEG-NH_2 into AuNP-PEG-GTA, we also tested one- and two-step conditions in PB and PBS 1×.[32] For the functionalization of AuNP with HS-PEG-NH_2 and their activation with GTA, 0.01% Tween 20 was useful, as its exclusion in either step resulted in losing particles as they adhered on the container. GTA in solution produces cyclic, dimeric, and/or polymeric reactive species that will crosslink all the reactants available.[33] By combining AuNP-PEG-NH_2, GTA, and $S_{461-493}$ in one-step, the intended AuNP-PEG-$S_{461-493}$ had similar properties than AuNP-PEG-GTA, indicating large amounts of unreacted peptide. In a two-step method, activating AuNP-PEG-NH_2 with GTA, followed by removal of excess GTA, and the addition of the $S_{461-493}$ peptide resulted in conjugates with properties distinguishable of the preceding intermediates (Figure 2, *B*).

Table 1
Physical properties of AuNP after their functionalization with HS-PEG-NH_2, activation with glutaraldehyde (GTA), and conjugation with $S_{461-493}$.

ID	λ_{max} (nm)	FWHM (nm)	d_H (nm)	PDI	ζ (mV)
AuNP (as-prep)	518	42	25.7	0.14	−38.
AuNP-PEG-NH_2	520	43	46.2	0.14	−1.1
AuNP-PEG-GTA	520	43	48.9	0.44	−6.2
AuNP-PEG-$S_{461-493}$	521	45	49.2	0.32	−8.4

After the functionalization of AuNP with HS-PEG-NH_2 and conjugation with peptide $S_{461-493}$, their visible spectrum red-shifted and broadened by 3 nm (Table 1). The ζ potential of AuNP-PEG-NH_2 became more negative once activated with GTA, and even more once conjugated with the negatively charged peptide $S_{461-493}$. The unchanged PDI indicated the stability of AuNP-PEG-NH_2 after the functionalization, while the increase and decrease in the PDI evidenced a lower stability after their reaction with the crosslinker GTA than after coupling with $S_{461-493}$. The AuNP-PEG-$S_{461-493}$ conjugate in PBS 1× with 0.01% Tween® 20 remained stable for months at 4 °C, requiring a minor agitation to resuspend.

After the functionalization of AuNP with HS-PEG-NH_2 the average radius measured by DLS increased 10 nm as the technique measures the equivalent hydrodynamic radius and is sensitive to the effect of capping. The contour length of PEG of M_n 5000 is between 31 and 40 nm, considering 113 subunits having a segment length of 0.318 ± 0.04 nm.[34] However, our measurements indicate PEG chains adopting random coil conformations when compared with an estimated end to end length of 8 nm that is based on Gaussian random coil models and experimental data with PEG of similar weight.[35]

After the activation with glutaraldehyde (GTA) and conjugation with peptide $S_{461-493}$ the hydrodynamic radius of AuNP-PEG-NH_2 increased a further 1.5 nm and remained within range. The contour length of peptide $S_{461-493}$ is 12 nm, the maximum extension assuming an average length of 0.36 nm per amino acid. However, the hydrodynamic radius of peptide $S_{461-493}$ estimated at 1.68 nm is in range with our measurements when compared with peptide sequences of 20, 30, and 40 amino acids with calculated hydrodynamic radii of 1.32, 1.61, and 1.79 nm, respectively.[36] The TEM analysis of AuNP-PEG-$S_{461-493}$ confirmed a mean diameter of 21.5 ± 7.1 nm, attributed to the AuNP (Figure 3).

More evidence on the effective modification and added stability post-functionalization of the AuNP was observed in electrophoresis, with similar remarks between batches prepared in different occasions. The as-prepared, citrate-coated AuNP aggregated irreversibly right after their deposition in the agarose

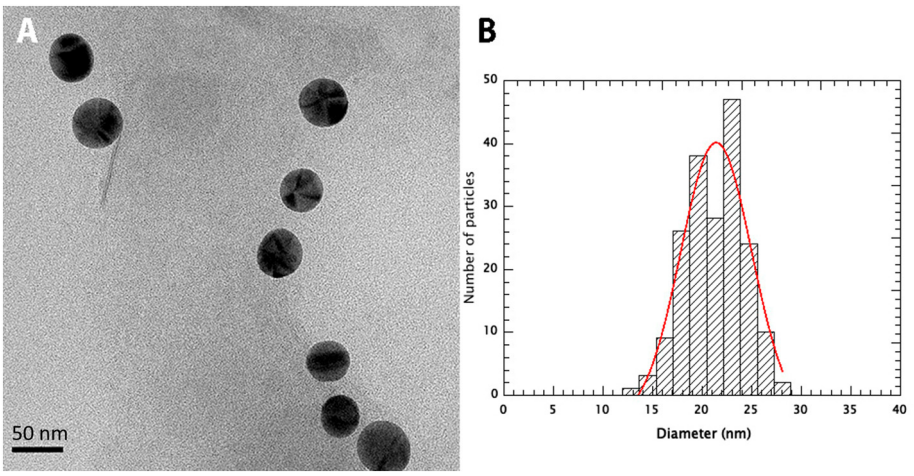

Figure 3. TEM analysis of AuNP-$S_{461\text{-}493}$. **(A)** Transmission electron microscopy of the AuNP-$S_{461\text{-}493}$ conjugate operated at 200 kV. The nanoparticles were deposited in carbon/formvar coated nickel grids and recorded using a Gatan 4 K camera. The scale bar is 50 nm. **(B)** Size distribution of the nanoparticles. The diameter of 188 particles was measured in two orthogonal directions and the size distribution was fitted to a Gaussian distribution (red line) centered at 21.5 nm with a width of 7.1 nm.

gel immersed in TA buffer, leaving a gray–purple stain that remained unaltered. AuNP-PEG-NH_2 migrated uniformly to the cathode due to the protonated amine, with most particles forming a compact block. AuNP-PEG-GTA remained in or near the well and slightly migrated to the anode due to the formation of enolate anions, with all particles arranged in a gradient due to expected reduced aldehydes. AuNP-PEG- $S_{461\text{-}493}$ migrated to the cathode given the charge of the peptide (−2, calculated), but diffusively due to the varying efficiency of the conjugation on each functionalized and activated AuNP (Figure 2, *B*, insert).

The AuNP-PEG-$S_{461\text{-}493}$ conjugate was formulated to provide 48 μg/mL of peptide available in the suspension. During the conjugation, the moles of peptide $S_{461\text{-}493}$ were calculated and added five times in excess, of which the equivalent to one monolayer of peptide shall react on the active surface of AuNP-PEG-GTA while the equivalent to four monolayers will not. Compared to controls containing 240 ± 7.4 μg/mL of peptide $S_{461\text{-}493}$ quantified by HPLC, the amount of peptide recovered after adding it to AuNP-PEG-GTA was 208.9 ± 5.2 μg/mL. These results indicate that the equivalent of 4.35 monolayers of unreacted peptide was recovered and quantified after the conjugation, and that the AuNP-PEG-$S_{461\text{-}493}$ conjugate contained 31.2 μg/mL of peptide.

Moderate toxicity of AuNP-$S_{461\text{-}493}$ in human cells in vitro

Assessing the toxicity in vitro of the nanoconjugates is relevant before starting in vivo evaluations. For this purpose, cell viability was determined by exposing a human cell line (HEK293-T) to AuNP-$S_{461\text{-}493}$. Upon a 48-h exposure to 12.5 μg/mL of AuNP-$S_{461\text{-}493}$, the cells did not exhibit a decrease in viability (99.5%) as determined by trypan blue staining (Figure 4, *A*), whereas treatments with 25 and 50 μg/mL induced a slight decrease (96.7% and 97.7%, respectively). The treatments leading to a modest decrease on viability were AuNP at 25 μg/mL (93.5%) and AuNP-$S_{461\text{-}493}$ at 250 μg/mL (94.9%). The resazurin assay revealed a slight gradual decrease on the metabolic activity upon exposure to increasing concentrations of either AuNP or AuNP-S461-493 in the 12.5-250 ug/mL range, however this effect was not statistically significant (Figure 4, *B*).

AuNP enhance the humoral response against $S_{461\text{-}493}$

Test mice groups were subjected to a sub-cutaneous (s.c.) immunization scheme to explore the capability of the AuNP carriers to enhance the immunogenicity of the $S_{461\text{-}493}$ peptide. An analysis of the anti-$S_{461\text{-}493}$ IgM response revealed an increase of this antibody isotype right after the first immunization with a ensuing decrease in the subsequent time points (Figure 5, *A*). In contrast, anti-$S_{461\text{-}493}$ IgG levels showed a gradual increase along the immunization scheme (Figure 5, *B*). Regarding the magnitude of the IgG response, the AuNP-$S_{461\text{-}493}$ conjugate induced a 4-fold increase in the antibody titers with respect to those induced by the $S_{461\text{-}493}$ peptide alone (Figure 6). Interestingly, the responses attained by the AuNP-$S_{461\text{-}493}$ conjugate were of the same magnitude to those induced by $S_{461\text{-}493}$ peptide emulsified in the Freund's adjuvant ($S_{461\text{-}493}$ + FA). The analysis of the IgG1 and IgG2a antibody subclasses revealed an overall predominance of the IgG1 subclass in all the experimental groups (Figure 7). The cytokine gene expression revealed an increase in the IFN-γ and IL-4 transcript levels in splenocytes from mice immunized with the AuNP-$S_{461\text{-}493}$ conjugate upon stimulation with the antigen ($S_{461\text{-}493}$), which supports the notion that the test vaccine is highly immunogenic, suggesting that both humoral and cellular responses are induced (Figure 8).

Discussion

Herein a prototype of a nanovaccine based on AuNP was generated as an effort to expand the possibilities for the development of rationally designed vaccines against SARS-CoV-2. It is well-known that nanosized materials, organic or inorganic, can lead to improved immunogenicity of antigens, which is especially important when the vaccine is formulated

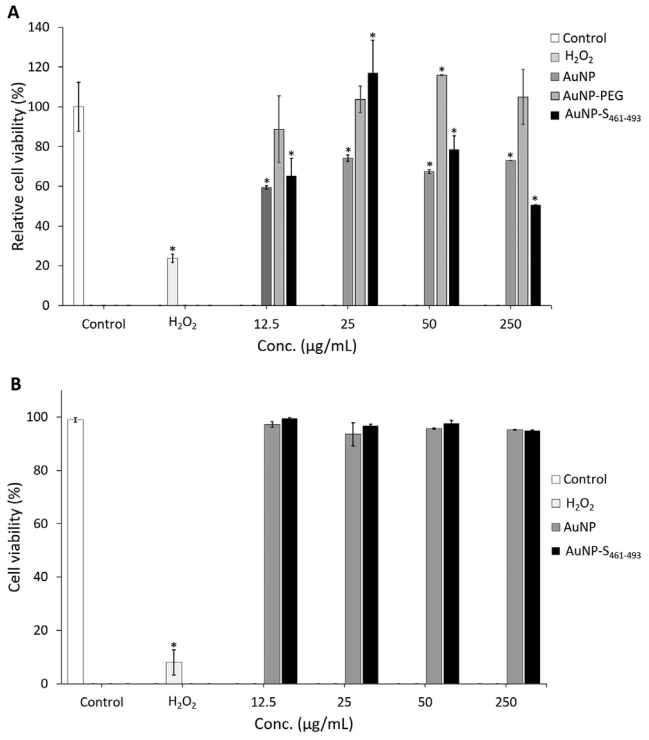

Figure 4. Toxicity assessment of the AuNP-$S_{461-493}$ conjugate. The effect of AuNP on cell viability was determined by incubating 1×10^5 cells with the respective treatment for 48 h. Cell viability was determined by trypan blue **(A)** or resazurin **(B)**. No difference in cell viability between the mock-treated samples (control) and any of the AuNP-treated samples was observed; the addition of the $S_{461-496}$ peptide on the AuNP did not change the cell viability. In contrast, the addition of H_2O_2 resulted in a cell viability of less than 10%. The asterisk indicates statistically significant differences versus the control.

with peptides that are typically poor immunogens. In particular, AuNP are considered biocompatible, noncytotoxic, and non-immunogenic entities, which make them highly attractive for biomedical applications that include the development of vaccines.[37] AuNP can act as carriers that exert immunodulator effects.[38–40]

We focused on the $S_{461-493}$ sequence, whose immunogenicity was first validated in sheep given the lack of experimental validation of protective epitopes from the protein S. This selection was guided by the in silico prediction of B cell epitopes and by the fact that the receptor binding domain (RBD) is recognized as a target of neutralizing antibodies in the case of SARS-CoV.[41,42] The selected $S_{461-493}$ peptide induced high levels of IgG (titers up to 60,000) under an immunization scheme of three months comprising the use of a strong adjuvant, confirming that $S_{461-493}$ carries a B cell epitope.

The synthesis of AuNP with a chemically pure salt of citric acid ensured the production of monodisperse, quasi-spherical, citrate-stabilized particles in one step, requiring no further treatment and remaining stable in solution for months, without changes in their properties. While AuNP produced with green materials such as plants, biopolymers, etc., would be considered safe for medical applications, it is recognized that more work is needed to commercialize and scale up their production.[43] Moreover, the existing formulations lead to obtain polydisperse particles, stabilized by a mixture of the various compounds from the biological source employed to carry out the reduction of the gold chloride precursor.

The functionalization of AuNP with either HS-PEG-COOH or HS-PEG-NH_2 provided not only steric and charge stabilization, but also two main options for the conjugation of the peptide, as its direct adsorption via the cysteine appended to the sequence $S_{461-493}$ failed due to its highly hydrophobic nature. The method to conjugate peptide $S_{461-493}$ on functionalized AuNP was developed after testing several conditions. The first chemistry tested, the usually reported conjugation method with EDC/NHS to activate AuNP-PEG-COOH and couple the peptide on it, tried as a one- or two-step reaction, resulted with evidence of mostly unreacted AuNP-PEG-COOH. The second method here proposed, with GTA crosslinking the Au-PEG-NH_2 and the primary amine of the peptide, resulted in conjugates with size and charge discernable from the simply functionalized AuNP and the activated ones, with a more contrasting difference when carrying the reaction in two steps rather than in one single step mixing all reactants. Overall, the optimization of the reaction conditions is critical since many experimental reports do not provide details on the coupling conditions leading to stable conjugates. In summary, the best condition we found was the functionalization of AuNP with HS-PEG-NH_2, followed by the activation with GTA and the removal of excess GTA prior the addition of peptide $S_{461-493}$ as described in Materials and Methods.

Before conducting the in vivo evaluation of the AuNP-$S_{461-493}$ conjugate, its safety was assessed in vitro using HEK293-T cells, revealing that the conjugate does not exert toxicity in the 12.5-250 μg/mL concentration range, which is in agreement with several studies validating the biocompatibility of AuNP.[44–46] We next explored the immunogenic properties of the AuNP-$S_{461-493}$ conjugate in test mice, with groups treated with the soluble peptide or the peptide co-administered with Freund's adjuvants as comparative controls. The induction of IgG responses was observed among the groups receiving the $S_{461-493}$ peptide in all test formulations, with a notably higher response in the group treated with the high dose of the AuNP-$S_{461-493}$ conjugate (mean titer = 1600) when compared to that observed for the group treated with an equivalent dose of the peptide alone (mean titer = 200). Interestingly, the magnitude of the response reached by the 5 μg dose of the AUNP-$S_{461-493}$ conjugate was similar in magnitude to that attained in the group co-administered with the Freund's adjuvant, which indicates that AuNP confer high immunogenicity to the $S_{461-493}$ peptide, surpassing the limitation of poor immunogenicity of the soluble peptide. The rate of IgG subclasses revealed a predominant IgG1 response, which suggests that the AuNP-$S_{461-493}$ conjugate induces a Th2 biased response. This response is favorable since the vaccine aims at inducing robust responses of neutralizing antibodies that could block the virus entry into the host cells.[47] In this respect, reports on AuNP-based vaccines targeting influenza virus and dengue virus have shown Th2 biased robust responses.[48,49]

The expression of IL-4 and IFN-γ is representative of the cellular and humoral responses, respectively. Their increased expression observed in splenocytes from mice immunized with the AuNP-$S_{461-493}$ conjugate upon stimulation with the target

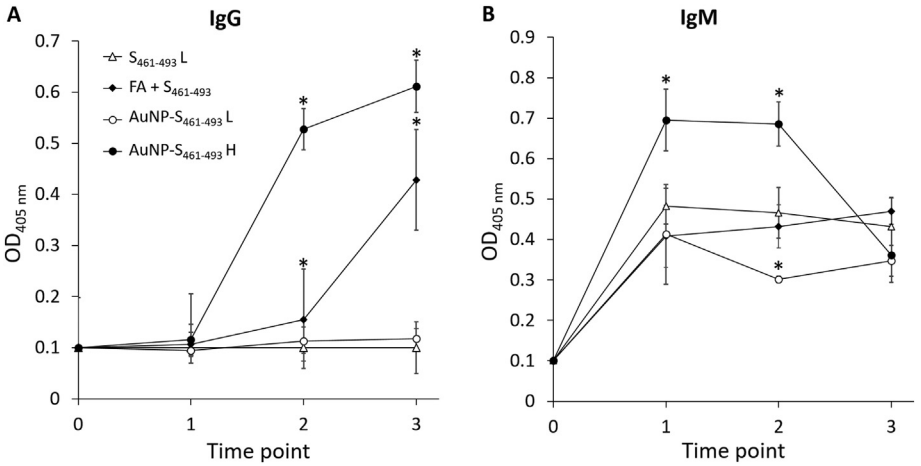

Figure 5. Evolution of IgM **(A)** and IgG **(B)** levels induced in mice against the $S_{461-493}$ peptide. Mice groups were s.c.-immunized on days 0, 14, and 21 with: 5 μg of the $S_{461-493}$ peptide diluted in PBS, the $S_{461-493}$ peptide plus complete Freund's adjuvant (+ FA; for priming, while for boosting the incomplete version was used), and a low (L) or a high (H) dose of AuNP-$S_{461-493}$, corresponding to 0.5 and 5 μg of $S_{461-493}$, respectively. Seric anti-$S_{461-493}$ antibody levels were determined on days 0, 13, 27, and 41 using test sera at a 1:200 dilution. The asterisk indicates statistically significant differences versus the antibody levels of the $S_{461-493}$ group.

$S_{461-493}$ antigen confirmed its high immunogenicity and suggests that this conjugate expanded populations of both Th2 and Th1 responses. However, further studies will be focused on determining in detail which immune mechanisms are behind the humoral response induced by AuNP-$S_{461-493}$.

In line with these findings, several viral antigens coupled to AuNP have shown marginal toxicity and an enhancement of the induced humoral responses. For instance, Li et al reported enhanced humoral responses against the E2 protein from the classical swine fever virus in s.c.-immunized mice.[50] The mechanism behind the adjuvant properties of AuNP is based on several investigations. It is proposed that the AuNP penetrate the extracellular matrix upon subcutaneous injection and reach the lymph nodes to be captured by antigen-presenting cell (APC) with the subsequent efficient induction of adaptive immune responses.[51] According to Zhang et al (2019), nanoparticles between 50 and 100 nm achieved higher delivery of antigen at the follicular dendritic cell dendrites (175-fold), enhancing humoral immune responses of germinal center B cell formation (5-fold), and higher antibody levels (5-fold) when compared to nanoparticles between 5 and 50 nm.[51]

Interestingly, Sekimukai et al (2020) reported the use of AuNP for vaccination against SARS-CoV using the full-length protein S, but while the AuNP-S conjugate showed high immunogenicity with similar effects when particles were in the 40-100 nm range, it did not lead to an increase in efficacy and a reduction on eosinophilic infiltration associated to the allergic inflammatory responses.[20] Therefore, even though AuNP are carriers that enhance the immune response, further approaches must direct the response to immune-relevant epitopes. Among the approaches to achieve this goal, the use of synthetic peptides covering those key epitopes is attractive to achieve robust, protective, and safe immune responses.[20] The perspectives for

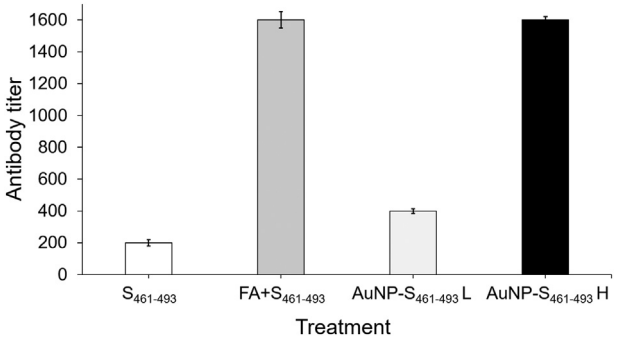

Figure 6. Adjuvant effect by AuNP carriers on the IgG response against $S_{461-493}$. Mice groups were s.c.-immunized on days 0, 14, and 21 with: 5 μg of the $S_{461-493}$ peptide diluted in PBS, the $S_{461-493}$ peptide plus complete Freund's adjuvant (+FA; for priming, while for boosting the incomplete version was used), and a low (L) or a high (H) dose of AuNP-$S_{461-493}$, corresponding to 0.5 and 5 μg of $S_{461-493}$, respectively. Anti-$S_{461-493}$ IgG titers were determined by ELISA using serial dilutions of test sera.

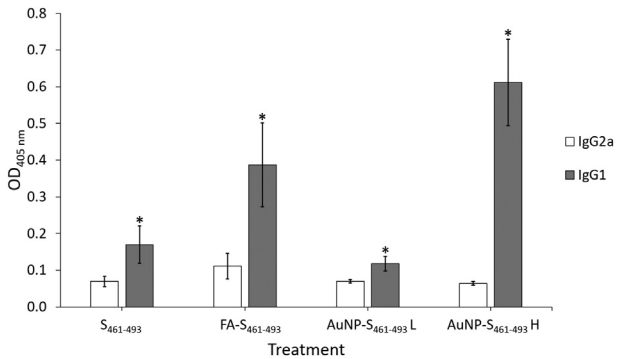

Figure 7. Analysis of the anti-$S_{461-493}$ IgG subclass abundance in test mice. Mice groups were s.c.-immunized on days 0, 14, and 21 with: 5 μg of the $S_{461-493}$ peptide diluted in PBS, the $S_{461-493}$ peptide plus complete Freund's adjuvant (+FA; for priming, while for boosting the incomplete version was used), and a low (L) or a high (H) dose of AuNP-$S_{461-493}$, corresponding to 0.5 and 5 μg of $S_{461-493}$, respectively. Anti-$S_{461-493}$ IgG1 or IgG2 seric levels were determined on by ELISA at a 1:200 dilution. The asterisk indicates statistically significant differences versus the IgG2a levels.

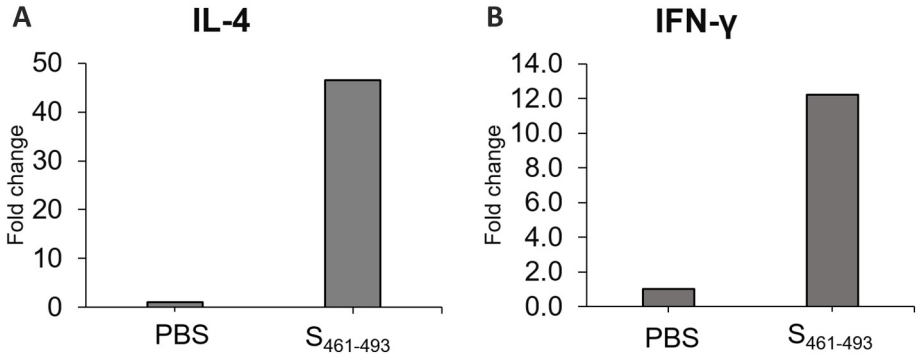

Figure 8. qPCR analysis for IL-4 and IFN-γ transcripts. The total RNA from splenocytes isolated from test mice immunized with the AuNP-$S_{461-493}$ immunogen and stimulated by the $S_{461-493}$ peptide was analyzed to determine the relative expression of IL-4 **(A)** and IFN-γ **(B)** transcripts. Data normalized by the amount of β-actin cDNA. Unstimulated cells were used as the control condition and the method was applied to determine the fold change expression.

this study contemplate the evaluation of the neutralizing potential of the induced immune response, expanding the number of target epitopes included in the formulation, and characterizing the mucosal immune response induced.

As long as the COVID-19 pandemic advances, the development of new immunization approaches against SARS-CoV-2 should be continued to favor the development of the next generation vaccines that could add to the vaccines that are expected to get approved in the midterm, increasing the potential to address the remarkable challenge of achieving global vaccination against this highly relevant emerging pathogen. In conclusion, this study opens the path for the formulation of epitope-based vaccines against SARS-CoV-2, which will be of high relevance in the development of the next generation vaccines against this and other emerging pathogens.

Author contribution statement

SRM: Conceptualization; Funding acquisition; Investigation; Supervision; Data curation; Project administration; Writing - original draft.

MJGS: Formal analysis; Methodology; Writing - original draft.

SFC: Methodology; Data curation; Writing - review & editing.

JIAV: Methodology; Data curation; Writing - review & editing.

MC: Methodology; Writing - original draft.

References

1. Dhama K, Khan S, Tiwari R, Sircar S, Bhat S, Malik YS, et al. Coronavirus disease 2019-COVID-19. *Clin Microbiol Rev* 2020;**33**(4): e00028 20https://doi.org/10.1128/CMR.00028-20.
2. Koirala A, Joo YJ, Khatami A, Chiu C, Britton PN. Vaccines for COVID-19: the current state of play. *Paediatr Respir Rev* 2020;**35**:43-9, https://doi.org/10.1016/j.prrv.2020.06.010.
3. Chakraborty R, Parvez S. COVID-19: an overview of the current pharmacological interventions, vaccines, and clinical trials. *Biochem Pharmacol* 2020;**180**:114184, https://doi.org/10.1016/j.bcp.2020.114184.
4. Wang N, Shang J, Jiang S, Du L. Subunit vaccines against emerging pathogenic human coronaviruses. *Frontiers Microbiol* 2020;**11**:298, https://doi.org/10.3389/fmicb.2020.00298.
5. Begum J, Mir NA, Dev K, Buyamayum B, Wani MY, Raza M. Challenges and prospects of COVID-19 vaccine development based on the progress made in SARS and MERS vaccine development. *Transbound Emerg Dis* 2020, https://doi.org/10.1111/tbed.13804.
6. Boopathi S, Poma AB, Kolandaivel P. Novel 2019 coronavirus structure, mechanism of action, antiviral drug promises and rule out against its treatment. *J Biomol Struct Dyn* 2020:1-10, https://doi.org/10.1080/07391102.2020.1758788.
7. Kim KD, Hwang I, Ku KB, Lee S, Kim SJ, Kim C. Progress and challenges in the development of COVID-19 vaccines and current understanding of SARS-CoV-2- specific immune responses. *J Microbiol Biotechnol* 2020;**30**(8):1109-15, https://doi.org/10.4014/jmb.2006.06006.
8. Amanat F, Krammer F. SARS-CoV-2 vaccines: status report. *Immunity* 2020;**52**(4):583-9, https://doi.org/10.1016/j.immuni.2020.03.007.
9. Prompetchara E, Ketloy C, Palaga T. Immune responses in COVID-19 and potential vaccines: lessons learned from SARS and MERS epidemic. *Asian Pac J Allergy Immunol* 2020;**38**(1):1-9, https://doi.org/10.12932/AP-200220-0772.
10. N. Cimolai, Defining protective epitopes for COVID-19 vaccination models. J Med Virol. (2020) 14:10.1002/jmv.25876. doi: https://doi.org/10.1002/jmv.25876.
11. Rosales-Mendoza S, Márquez-Escobar VA, González-Ortega O, Nieto-Gómez R, Arévalo-Villalobos JI. What does plant-based vaccine technology offer to the fight against COVID-19? *Vaccines (Basel)* 2020;**8**(2):183, https://doi.org/10.3390/vaccines8020183.
12. Salazar-González JA, González-Ortega O, Rosales-Mendoza S. Gold nanoparticles and vaccine development. *Expert Rev Vaccines* 2015;**14**(9):1197-211, https://doi.org/10.1586/14760584.2015.
13. Carabineiro SAC. Applications of gold nanoparticles in nanomedicine: recent advances in vaccines. *Molecules* 2017;**22**(5):857, https://doi.org/10.3390/molecules22050857.
14. Das S, Debnath N, Mitra S, Datta A, Goswami A. Comparative analysis of stability and toxicity profile of three differently capped gold nanoparticles for biomedical usage. *Biometals* 2012;**25**(5):1009-22, https://doi.org/10.1007/s10534-012-9567-1.
15. Niikura K, Matsunaga T, Suzuki T, Kobayashi S, Yamaguchi H, Orba Y, et al. Gold nanoparticles as a vaccine platform: influence of size and shape on immunological responses in vitro and in vivo. *ACS Nano* 2013;**7**:3926-38, https://doi.org/10.1021/nn3057005.
16. Fytianos K, Rodriguez-Lorenzo L, Clift MJ, Blank F, Vanhecke D, von Garnier C, et al. Uptake efficiency of surface modified gold nanoparticles does not correlate with functional changes and cytokine secretion in human dendritic cells in vitro. *Nanomedicine* 2015;**11**:633-44, https://doi.org/10.1016/j.nano.2014.11.004.
17. Zhou Q, Zhang Y, Du J, Li Y, Zhou Y, Fu Q, et al. Different-sized gold nanoparticle activator/antigen increases dendritic cells accumulation in

liver-draining lymph nodes and CD8+ t cell responses. *ACS Nano* 2016;**10**:2678-92, https://doi.org/10.1021/acsnano.5b07716.
18. le Guével X, Palomares F, Torres MJ, Blanca M, Fernandez TD, Mayorga C. Nanoparticle size influences the proliferative responses of lymphocyte subpopulations. *RSC Adv* 2015;**5**:85305-9, https://doi.org/10.1039/c5ra16164a.
19. Alizadeh F, Khodavandi A. Systematic review and meta-analysis of the efficacy of nanoscale materials against coronaviruses—possible potential antiviral agents for SARS-CoV-2. *IEEE Trans Nanobioscience* 2020;**19**(3):485-97, https://doi.org/10.1109/TNB.2020.2997257.
20. Sekimukai H, Iwata-Yoshikawa N, Fukushi S, Tani H, Kataoka M, Suzuki T, et al. Gold nanoparticle-adjuvanted S protein induces a strong antigen-specific IgG response against severe acute respiratory syndrome-related coronavirus infection, but fails to induce protective antibodies and limit eosinophilic infiltration in lungs. *Microbiol Immunol* 2020;**64**(1):33-51, https://doi.org/10.1111/1348-0421.12754.
21. Sanchez-Villamil JI, Tapia D, Torres AG. Development of a gold nanoparticle vaccine against enterohemorrhagic Escherichia coli O157: H7. *mBio* 2019;**10**(4):e01869 19https://doi.org/10.1128/mBio.01869-19.
22. Vetro M, Safari D, Fallarini S, Salsabila K, Lahmann M, Penadés S, et al. Preparation and immunogenicity of gold glyco-nanoparticles as antipneumococcal vaccine model. *Nanomedicine* 2017;**12**(1):13-23, https://doi.org/10.2217/nnm-2016-0306.
23. Nikaeen G, Abbaszadeh S, Yousefinejad S. Application of nanomaterials in treatment, anti-infection and detection of coronaviruses. *Nanomedicine* 2020;**15**(15):1501-12, https://doi.org/10.2217/nnm-2020-0117.
24. Arevalo-Villalobos JI, Govea Alonso DO, Rosales-Mendoza S. Using carrot cells as biofactories and oral delivery vehicles of LTB-Syn: a low-cost vaccine candidate against synucleinopathies. *J Biotechnol* 2020 Feb 10;**309**:75-80.
25. Xia H, Bai S, Hartmann J, Wang D. Synthesis of monodisperse quasi-spherical gold nanoparticles in water via silver(I)-assisted citrate reduction. *Langmuir* 2010;**26**(5):3585-9.
26. K. Rahme, L. Chen, R. Hobbs, M. Morris, C. O'Driscoll C, Holmes J, PEGylated gold nanoparticles: polymer quantification as a function of PEG lengths and nanoparticle dimensions. RSC Adv, 2013, 3, 6085–6094.
27. Bartczak D, Kanaras A. Preparation of peptide-functionalized gold nanoparticles using one pot EDC/sulfo-NHS coupling. *Langmuir* 2011;**27**:10119-23.
28. Rao X, Lai D, Huang X. A new method for quantitative real-time polymerase chain reaction data analysis. *J Comput Biol* 2013;**20**(9):703-11, https://doi.org/10.1089/cmb.2012.0279.
29. Bastús N, Sánchez-Tilló E, Pujals S, Farrera C, López C, Giralt E, et al. Homogeneous conjugation of peptides onto gold nanoparticles enhances macrophage response. *ACS Nano* 2009;**3**(6):1335-44.
30. Almeida J, Lin A, Figueroa E, Foster A, Drezek R. In vivo gold nanoparticle delivery of peptide vaccine induces anti-tumor immune response in prophylactic and therapeutic tumor models. *Small* 2015;**11**(12):1453-9.
31. Busch R, Karim F, Weis J, Sun Y, Zhao C, Vasquez E. Optimization and structural stability of gold nanoparticle-antibody bioconjugates. *ACS Omega* 2019;**4**:15269-79.
32. Carter J. In: Walker J, editor. *Conjugation of peptides to carrier proteins via glutaraldehyde. The protein protocols handbook*. New Jersey: Humana Press; 1996.
33. Bioconjugate Hermanson G. *Techniques. 3rd edition*. London: Academic Press; 2013.
34. Oesterhelt F, Rief M, Gaub H. Single molecule force spectroscopy by AFM indicates helical structure of poly(ethylene-glycol) in water. *New J Phys* 1999;**1**(1):6.
35. Manson J, Kumar D, Meenan B, Dixon D. Polyethylene glycol functionalized gold nanoparticles: the influence of capping density on stability in various media. *Gold Bulletin* 2011;**44**:99-105.
36. Nygaard M, Kragelund B, Papaleo E, Lindorff-Larsen K. An efficient method for estimating the hydrodynamic radius of disordered protein conformations. *Biophys J* 2017;**113**:550-7.
37. Shukla R, Bansal V, Chaudhary M, Basu A, Bhonde RR, Sastry M. Biocompatibility of gold nanoparticles and their endocytotic fate inside the cellular compartment: a microscopic overview. *Langmuir* 2005;**21**(23):10644-54, https://doi.org/10.1021/la0513712.
38. Zhang X. Gold nanoparticles: recent advances in the biomedical applications. *Cell Biochem Biophys* 2015;**72**(3):771-5, https://doi.org/10.1007/s12013-015-0529-4.
39. Dykman LA, Khlebtsov NG. Immunological properties of gold nanoparticles. *Chem Sci* 2017;**8**(3):1719-35, https://doi.org/10.1039/c6sc03631g.
40. Surendran SP, Moon MJ, Park R, Jeong YY. Bioactive nanoparticles for cancer immunotherapy. *Int J Mol Sci* 2018;**19**(12):3877, https://doi.org/10.3390/ijms19123877.
41. A.M. Baig, A. Khaleeq, H. Syeda, Elucidation of cellular targets and exploitation of the receptor-binding domain of SARS-CoV-2 for vaccine and monoclonal antibody synthesis. J Med Virol. (2020) https://doi.org/10.1002/jmv.26212. doi: https://doi.org/10.1002/jmv.26212.
42. Corrêa CG, Laaksonen A, Barroso da Silva FL. On the interactions of the receptor-binding domain of SARS-CoV-1 and SARS-CoV-2 spike proteins with monoclonal antibodies and the receptor ACE2. *Virus Res* 2020;**285**:198021, https://doi.org/10.1016/j.virusres.2020.198021.
43. Lee KX, Shameli K, Yew YP, Teow SY, Jahangirian H, Moghaddam RR, et al. Recent developments in the facile bio-synthesis of gold nanoparticles (AuNP) and their biomedical applications. *Int J Nanomedicine* 2020;**15**:275-300.
44. Lee E, Jeon H, Lee M, Ryu J, Kang C, Kim S, et al. Molecular origin of AuNP-induced cytotoxicity and mechanistic study. *Sci Rep* 2019;**9**:1-13.
45. Manivasagan P, Oh J. Marine polysaccharide-based nanomaterials as a novel source of nanobiotechnological applications. *Int J Biol Macromol* 2016;**82**:315-27.
46. Woźniak-Budych MJ, Langer K, Peplińska B, Przysiecka Ł, Jarek M, Jarz bski M, et al. Copper-gold nanoparticles: fabrication, characteristic and application as drug carriers. *Mater Chem Phys* 2016;**179**:242-53.
47. Huang AT, Garcia-Carreras B, Hitchings MDT, Yang B, Katzelnick LC, Rattigan SM, et al. A systematic review of antibody mediated immunity to coronaviruses: kinetics, correlates of protection, and association with severity. *Nat Commun* 2020;**11**(1):4704.
48. Quach QH, Ang SK, Chu JJ, Kah JCY. Size-dependent neutralizing activity of gold nanoparticle-based subunit vaccine against dengue virus. *Acta Biomater* 2018;**78**:224-35.
49. Tao W, Gill HS. M2e-immobilized gold nanoparticles as influenza A vaccine: role of soluble M2e and longevity of protection. *Vaccine* 2015;**33**(20):2307-15.
50. Li Y, Jin Q, Ding P, Zhou W, Chai Y, Li X, et al. Gold nanoparticles enhance immune responses in mice against recombinant classical swine fever virus E2 protein. *Biotechnol Lett* 2020;**42**(7):1169-80, https://doi.org/10.1007/s10529-020-02853-w.
51. Zhang YN, Lazarovits J, Poon W, Ouyang B, Nguyen LNM, Kingston BR, et al. Nanoparticle size influences antigen retention and presentation in lymph node follicles for humoral immunity. *Nano Lett* 2019;**19**(10):7226-35.